Faraday Discussions

Accepted Manuscript

This manuscript will be presented and discussed at a forthcoming Faraday Discussion meeting. All delegates can contribute to the discussion which will be included in the final volume.

Register now to attend! Full details of all upcoming meetings: http://rsc.li/fd-upcoming-meetings

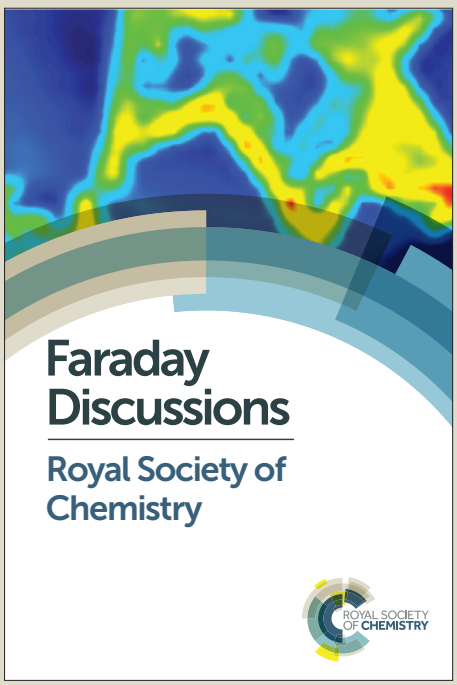

This is an *Accepted Manuscript*, which has been through the Royal Society of Chemistry peer review process and has been accepted for publication.

Accepted Manuscripts are published online shortly after acceptance, before technical editing, formatting and proof reading. Using this free service, authors can make their results available to the community, in citable form, before we publish the edited article. We will replace this *Accepted Manuscript* with the edited and formatted *Advance Article* as soon as it is available.

You can find more information about *Accepted Manuscripts* in the Information for Authors.

Please note that technical editing may introduce minor changes to the text and/or graphics, which may alter content. The journal's standard Terms & Conditions and the Ethical guidelines still apply. In no event shall the Royal Society of Chemistry be held responsible for any errors or omissions in this *Accepted Manuscript* or any consequences arising from the use of any information it contains.

ROYAL SOCIETY OF CHEMISTRY

www.rsc.org/faraday_d

Journal Name

ARTICLE TYPE

Cite this: DOI: 10.1039/xxxxxxxxxx

Magnetic filament brushes: tuning the properties of a magnetoresponsive supracolloidal coating†

Pedro A. Sánchez,*[a] Elena S. Pyanzina,[b] Ekaterina V. Novak,[b] Joan J. Cerdà,[c] Tomàs Sintes,[c] and Sofia S. Kantorovich[a,b]

Received Date
Accepted Date

DOI: 10.1039/xxxxxxxxxx

www.rsc.org/journalname

We present a theoretical study on the design of a supramolecular magnetoresponsive coating. The coating is formed by a relatively dense array of supracolloidal magnetic filaments grafted to a surface in a polymer brush-like arrangement. In order to determine and optimise the properties of the magnetic filament brush, we perform extensive computer simulations with a coarse-grained model that takes into account the correlations between the magnetic moments of the particles and the backbone crosslinks. We show that the self-assembly of magnetic beads from neighbouring filaments defines the equilibrium structural properties of the complete brush. In order to control this self-assembly, we highlight two external stimuli that can lead to significant effects: temperature of the system and an externally applied magnetic field. Our study reveals self-assembly scenarios inherently driven by the crosslinking and grafting constraints. Finally, we explain the mechanisms of structural changeovers in the magnetic filament brushes and confirm the possibility to control them by changing the temperature or the intensity of an external magnetic field.

1 Introduction

Self-assembly—the reorganisation of the components of a system into patterns or defined structures driven by their interactions—is a ubiquitous mechanism in many physical systems, as well as a key tool of increasing importance in the bottom-up design of materials and nanotechnologies.[1] As the knowledge of the self-assembly properties of simple systems grows, more complex components and strategies can be explored. In particular, the creation of sophisticated structures by means of the hierarchical self-assembly of their components—or building blocks—has experienced great development in recent years.[2] In this strategy, the self-assembly of the final structure takes place in multiple steps. Each step produces building blocks of increasing complexity, which are able to self-assemble into new structures in the next step. One of the current leading goals of hierarchical self-assembly techniques, particularly in the context of soft matter systems, is the creation of stimuli-responsive materials, *i.e.*, materials that experience a controlled change in their properties as a response to external drive.[3]

Among the different materials with relevant self-assembly properties available, magnetic colloids have attracted a great interest in recent years due to their broad potential as basic building blocks of novel responsive materials and nanotechnologies.[4–6] Under adequate conditions, simple spherical magnetic colloids dispersed in a carrier fluid self-assemble into chains, rings and branched structures driven by the non-central character of the interparticle magnetic dipole-dipole interaction that favours the head-to-tail orientation of the neighbouring magnetic moments.[7,8] The self-assembly into chains with the head-to-tail orientation of the dipoles can also be stimulated by an applied external magnetic field. These magnetically-driven self-assembly processes lead to significant changes in the macroscopic behaviour of these systems: their overall magnetic response, rheology and thermodynamics depend strongly on the microstructure of magnetic soft matter.[9–11]

Besides their direct self-assembly, magnetic colloids play an increasingly important part in the development of new responsive and functional nanocomposite materials, particularly in combi-

[a] *University of Vienna, Sensengasse 8, 1090 Vienna, Austria. E-mail: pedro.sanchez@univie.ac.at*
[b] *Ural Federal University, Lenin av. 51, 620000 Ekaterinburg, Russia.*
[c] *Instituto de Física Interdisciplinar y Sistemas Complejos (CSIC-UIB), E-07122 Palma de Mallorca, Spain.*

nation with polymer molecules.[12,13] In general, the coating of colloidal particles with polymers is a technique frequently used to stabilise and/or functionalise their surfaces. Such polymeric coatings can also be used to permanently crosslink the individual colloids that form a self-assembled cluster, stabilising the overall structure and preventing their disaggregation even when the system is no longer under the proper self-assembly conditions. In the case of magnetic colloids, their self-assembled head-to-tail chains have been made permanent by polymer crosslinking since more than a decade.[14] The result of this crosslinking is a semiflexible chain with a polymer-like supracolloidal structure, with the magnetic colloids playing the role of polymer monomers. The control of the properties of these systems, known as magnetic filaments, has experienced a great progress in recent years thanks to the enhancement of crosslinking techniques.[15–18]

Recently, we proposed the use of magnetic filaments in order to create a magnetoresponsive thin film surface.[19] The basic idea of our approach is to replace, with magnetic filaments, the densely end-grafted polymer chains that form a polymer brush.[20,21] In general, polymer brushes are widely used for the creation of stimuli-responsive surfaces[3,22] but, except for few compounds at very extreme conditions, polymer molecules are unable to provide significant responses to external magnetic fields. The control of the properties of a surface by means of magnetic fields is particularly interesting in soft matter systems, where other parameters—like pH or electric fields—have strong and complex interactions with most substances of interest, making the control of their effects more difficult. For these reasons, efforts have been recently made to create magnetoresponsive polymer brush structures by embedding magnetic colloids within the polymer array.[23,24] On the other hand, magnetic filaments with one end grafted to a surface, either individually or in sparse arrays, have been largely studied as micro- and nanofluidic actuators, pumpers or propellers.[25–30] In our case, we analyse the result of increasing the grafting density of tethered magnetic filaments to form a polymer brush-like structure at a supracolloidal scale. In a preliminary study,[19] we showed that this system shows a significantly more pronounced structural equilibrium response to an external field than former systems of polyelectrolyte brushes with extended electric dipoles,[31] or than the aforementioned polymer brushes with embedded magnetic colloids.[23,24] Our preliminary results also indicated that the origin of such strong structural response should be attributed to the particular self-assembly properties of the crosslinked colloids placed in the highly constrained environment of the brush structure.

Here, we aim to pinpoint the intrinsic mechanisms responsible for overall equilibrium structural properties of magnetic filament brushes. This understanding will provide the opportunity to control the thickness and the local density of the brush—the two most important features of a coating—with external stimuli. In contrast to our previous work, in the present study we focus on the influence of temperature and external field on the self-assembly of magnetic beads from neighbouring filaments. Self-assembly proves to be the key to manipulate the responses of the filament brushes, because these are the topology and the sizes of the formed clusters who define the local magnetic properties and reflect the balance between the entropy and the dipolar correlations.

2 Model and Methods

2.1 Magnetic Filament Brush Model

In our polymer brush-like system of supracolloidal magnetic filaments, we consider the latter to be formed by spherical single-domain ferromagnetic colloids that keep the orientation of their magnetic moments—described as simple point dipoles—fixed in one of the directions of the magnetic easy axis of the particle. These particles are considered to have high enough internal anisotropy and large enough volume to be be above the superparamagnetic regime. The polymer crosslinkers that keep the chain-like structure of these filaments are assumed to be attached to the surface of the colloids at the projection points of such easy axes. This combination corresponds to experimental magnetic filaments created by crosslinking single-domain colloids of strong ferromagnetic materials after their self-assembly into straight chains, with a head-to-tail arrangement of their magnetic moments. Therefore, the equilibrium structures of these filaments will tend to keep a nearly head-to-tail orientation of the dipoles between close neighbours along the chain. In order to model this type of magnetic filaments, we recently introduced a coarse-grained, bead-spring model that takes into account the coupling between the orientation of the magnetic dipoles and the chain backbone, led by the crosslinkers.[32,33] In this model, the magnetic colloids are represented as soft spherical beads, with a characteristic diameter d. The soft-core steric repulsion between such spheres is given by a WCA potential[34]

$$U_{\mathrm{WCA}}(r) = \begin{cases} U_{\mathrm{LJ}}(r) - U_{\mathrm{LJ}}(r_{\mathrm{cut}}), & r < r_{\mathrm{cut}} \\ 0, & r \geq r_{\mathrm{cut}} \end{cases}, \qquad (1)$$

where r is the centre-to-centre distance between the spheres, $U_{\mathrm{LJ}}(r)$ is the conventional Lennard-Jones potential,

$$U_{\mathrm{LJ}}(r) = 4\varepsilon_s[(d/r)^{12} - (d/r)^6], \qquad (2)$$

and $r_{\mathrm{cut}} = 2^{1/6}d$ is a shift that makes the potential purely repulsive. In addition, each soft sphere carries a point magnetic dipole at its centre, $\vec{\mu}$, which leads to a conventional magnetic dipole-dipole interaction between the beads:

$$U_{dd}(i,j) = \frac{\vec{\mu}_i \cdot \vec{\mu}_j}{r^3} - \frac{3\,(\vec{\mu}_i \cdot \vec{r})\,(\vec{\mu}_j \cdot \vec{r})}{r^5}, \qquad (3)$$

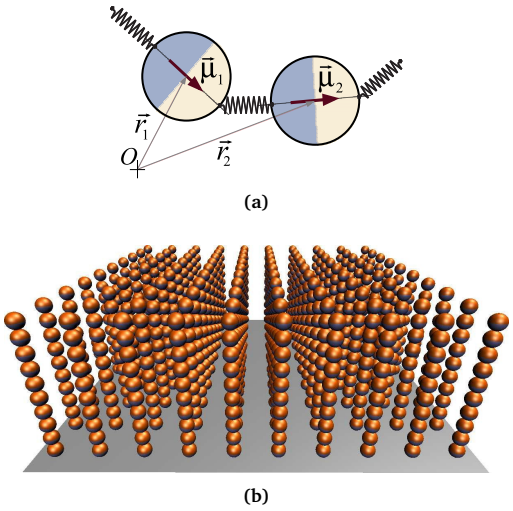

Fig. 1 (a) Sketch of the magnetic filament model. Magnetic beads are represented as two-colour spheres, indicating the orientation of the dipoles. Crosslinkers are represented as springs. (b) Example of a magnetic filament brush used as an initial configuration in our computer simulations, corresponding to a grafting density of $\sigma = 0.111$ of filaments formed by $N = 10$ beads.

where $\vec{r} = \vec{r}_i - \vec{r}_j$ is the centre-to-centre displacement vector between the beads i and j, which have dipolar moments $\vec{\mu}_i$ and $\vec{\mu}_j$ respectively. If a uniform external magnetic field, $\vec{H}$, is applied to the system, each magnetic dipole $\vec{\mu}_i$ will experience an interaction that tends to align it with the field. The energy of such dipole-field interaction has the form:

$$U_H(i) = -\vec{\mu}_i \cdot \vec{H}. \tag{4}$$

In order to mimic the coupling between the orientation of the dipoles and the chain backbone introduced by the crosslinkers, we use the following attractive potential between any pair of crosslinked neighbours, which depends on both the centre-to-centre displacement vector between them, $\vec{r}$, and on the relative orientation of their dipoles:

$$U_S(i,j) = \frac{1}{2} K_S \left(\vec{r} - (\hat{\mu}_i + \hat{\mu}_j) \frac{d}{2} \right)^2, \tag{5}$$

where $\hat{\mu}_i = \vec{\mu}_i / |\vec{\mu}_i|$ and $\hat{\mu}_j = \vec{\mu}_j / |\vec{\mu}_j|$ are the unitary vectors parallel to each associated dipole moment. Expression (5) corresponds essentially to a harmonic spring potential that connects the surfaces of a pair of bonded particles at the projection points of the dipole head of one of them and the dipole tail of the other. The strength of the attraction is defined by the prefactor K_S. The combination of potentials (1) and (5) provides the actual bonding interaction between the neighbouring beads in the filament. Figure 1a shows a sketch of the described magnetic filament model.

Finally, in order to create a polymer brush-like structure, we arrange a relatively dense array of magnetic filaments—formed by N identical beads—tethered by one of their ends to a flat sterically repulsive surface in the XY plane. In particular, the grafting of each filament is achieved by fixing the position of its tethered end bead next to the surface, with the corresponding dipole permanently pointing perpendicular to the latter. The grafting positions are distributed in a square lattice arrangement with a separation constant a. This gives a number grafting density—*i.e.*, the number of grafting points per unit of surface area—of $\sigma = a^{-2}$. In the initial configuration of the system, the filaments are placed as completely straight chains perpendicular to the grafting surface. Figure 1b shows an example of the initial configurations of magnetic filament brushes used in this study. The steric repulsion produced by the grafting surface on the filament beads is given by a truncated shifted 9-3 Lennard-Jones potential,[35] which is obtained by applying expression (1) to

$$U_{\mathrm{LJ}}^{9-3}(r) = \frac{3\sqrt{3}}{2} \left[\left(\frac{d}{2r} \right)^9 - \left(\frac{d}{2r} \right)^3 \right], \tag{6}$$

where r is the distance between the centre of the bead and the surface. This potential is the result of integrating a conventional 12-6 Lennard-Jones potential over an infinite plane.

2.2 Simulation and Analysis Approaches

Our characterisation of the equilibrium properties of supracolloidal magnetic filament brushes is based on two main methods: first, we performed extensive computer simulations with the phenomenological model described above; second, we analysed the simulation results by means of a combination of conventional parameters—in the context of studies on polymer brush systems—and a detailed characterisation of the brush internal structure obtained by means of graph-theory techniques.

The simulation method we used is molecular dynamics in the canonical ensemble. In particular, we used a Langevin thermostat in order to treat implicitly the effects of the thermal fluctuations of the background fluid on the filament beads.[36] A pseudo-infinite brush system was mimicked by imposing lateral periodic boundaries. Efficient calculation of the long-range magnetic interactions under these conditions is rather difficult. To address this issue, we used the approximate dipolar-P^{3}M method,[37] in combination with the dipolar Layer Correction method,[38] that takes into account the slab geometry of the system. All the simulations were carried out with the ESPResSo 3.2.0 simulation package.[39,40] Further details of the simulation method can be found in our introductory work on this system.[19]

The analysis of simulation results for the equilibrium configurations of the filament brushes was done in two different ways. First, we calculated two traditional parameters used to characterise the overall structure of polymer brush-like systems: the ver-

tical density profile, $\phi(z^*)$, and the average height, $\langle z^* \rangle$. $\phi(z^*)$ is simply defined as the number density distribution of the centres of the filament beads as a function of the reduced distance to the grafting surface, $z^* = z/d(N-1)$, where $d(N-1)$ is the contour length of the filaments measured in units of the bead characteristic diameter. The average height is obtained as the first moment of the density profile:

$$\langle z^* \rangle = \frac{1}{d(N-1)} \frac{\int_0^\infty \phi(z)\, z\, dz}{\int_0^\infty \phi(z)\, dz}. \quad (7)$$

The second analysis approach is based on the fact that the peculiar behaviour that we observed in the aforementioned collective parameters for different values of both temperature and external magnetic field, can be only explained by the existence of characteristic arrangements of the dipolar beads within the brush. In other words, the overall response of the filament brush to the external control parameters is determined by the self-assembly properties of the individual magnetic colloids under the geometrical constrains imposed by three factors: their belonging to a permanent chain; the presence of the neighbouring chains; the grafting surface. In order to characterise such self-assembly properties, we used an analysis approach based on graph theory.[41] In this approach, which we introduced in our preliminary work on magnetic filament brushes,[19] we study the arrangements of the beads by introducing the concept of generic connections between them. In particular, we consider two beads to be connected if their centre-to-centre distance does not exceed a certain threshold. Once all the connections in the system have been determined according to such simple criterium, the brush structure can be represented as a graph in which the dipolar beads are the vertices and the connections between them are the edges. A statistical analysis of the brush structure can be then performed by means of different graph parameters and their distributions for different conditions. The parameters analysed here are the distribution of edges, the vertex degree, the cluster size and the betweenness centrality. The vertex degree, δ, is the number of edges of a given vertex. To define the cluster size and the centrality, it is required to introduce the concepts of path, cluster and shortest path. A path between two given vertices, u and w, is any trajectory along the edges of the graph, p_{uw}, that connects such vertices, either directly or by crossing any number of other vertices. A cluster is a maximal set of vertices for which there exists at least one path that connects any pair of them, and its size is the number of vertices it has. Finally, a shortest path between vertices u and w, p^s_{uw}, is any path p_{uw} that crosses the minimum possible number of intermediate vertices. According to these definitions, the betweenness centrality of a given vertex v that belongs to a cluster V is defined as

$$C_B(v) = \sum_{u,w \in V} \frac{p^s_{uw}(v)}{p^s_{uw}}, \quad (8)$$

where p^s_{uw} is the total number of shortest paths between each pair of vertices u and w that belong to the cluster V, and $p^s_{uw}(v)$ is the number of those paths that pass through v. Therefore, $C_B(v)$ is a measure of the importance in terms of optimal path construction of the vertex v in the cluster.

3 Results and Discussion

For simplicity, here we measure all the physical parameters in reduced units, taking as reference the characteristic diameter of the colloids, $d = 1$, their mass $m = 1$, and the prefactor of the soft-core steric potential (1) and (2), $\varepsilon_s = 1$. The prefactor of the potential (5) is set to $K_s = 30$, a value that, according to our previous studies with this model of magnetic filaments,[19,32,33] provides an average distance between bonded beads—or average bond length, $\langle b \rangle$—close to the reference bead soft core diameter, $\langle b \rangle \sim d = 1$. However, it is important to note that the bond length is not fixed: since the attractive part of the bonding interaction (5) is an unbounded harmonic potential, the bond length experiences thermal fluctuations by effect of the temperature. Therefore, its average value tends to grow as the temperature is increased.[33] For the parameters used in this study, the maximum distance between the surfaces of two bonded beads was approximately $d/2$. Finally, we have taken $\mu^2 = (\vec{\mu} \cdot \vec{\mu}) = 5$ for the squared dipole moment of the beads. We explored the equilibrium structures of the magnetic filament brushes for two sets of values of the control parameters. In one case, we analysed the effects of variations in temperature at zero field by taking a range of reduced temperatures within $T = 0.35$ and $T = 5$. In the other case, the effect of an external magnetic field perpendicular to the grafting surface at a reference reduced temperature $T = 1$ has been studied by varying its modulus from $H = 0.5$ to $H = 4$. In both cases, a single filament length of $N = 10$ and two grafting densities, $\sigma = 0.040$ and $\sigma = 0.111$, were chosen.

The set of parameters we described above can be associated with various experimental systems. Let $T = 1$ correspond to 300 K. As an example, we can choose magnetite with a bulk saturation magnetisation at this temperature equal to 450 kA/m. To reach the value $\mu^2 = 5$ at close contact, the diameter of the nanoparticle magnetic core should be approximately 30 nm.[7] With this magnetic core size, the thickness of the nonmagnetic layer on the particle surface can be estimated to be on the order of 3 nm. To keep the distance between the centres of the crosslinked nanoparticles at approximately 50 nm, one needs the crosslinking polymers to be at least 7 nm in length, which corresponds to approximately 20 DNA base pairs.[42,43] Varying the temperature in experiment is not directly equivalent to that in simulations, as the absolute value of the saturation magnetisation in real ferromagnetic materials is temperature-dependent. In other words, the range of dimensionless temperatures chosen in our simulations is supposed to reflect the variation of the ratio between the magnetic and ther-

mal energies. Besides that, if the temperature becomes too low in experiment, the system might undergo undesirable phase transformations such as carrier liquid freezing or irreversible coagulation due to the loss of colloidal stability. However, it is experimentally possible to keep the suspension of magnetite nanoparticles stable down to 150 K,[44,45] which in our simulations corresponds to a value between $T = 0.35$ and $T = 0.75$.

3.1 Effects of Temperature

It is known that the self-assembled structures of free magnetic colloids in suspension experience diverse structural transitions on cooling.[10,11] Computer simulations have also provided indications of structural changes in isolated magnetic filaments as the importance of the thermal fluctuations decreases in front of the dipole-dipole interactions.[32,46] In magnetic filament brushes, the effects of the added geometrical restrictions and the crowded environment make the structural changes, which these systems may experience as a function of the temperature, hard to anticipate.

We begin the analysis of the effects of temperature on the equilibrium structure of the magnetic filament brush at zero field by examining the evolution of the density profiles, $\phi(z^*)$, and the average brush height, $\langle z^* \rangle$. Figure 2 shows the results obtained for these parameters. The density profiles (Figure 2a) evidence the highly compact overall structure of the magnetic brush, showing a rather abrupt decay of the density in the upper regions, as was discussed in our previous work for the case $T = 1$.[19] Here, we can see that this behaviour persists for both grafting densities within the whole range of explored temperatures, and becomes notably more pronounced as T decreases. At low temperatures, practically all the beads remain close to the grafting surface—within a region below 1/2 of the contour length of the filaments—whereas the decay of the profile above such region is extremely abrupt. Interestingly, at low temperatures the profiles for both grafting densities are very similar. As the temperature increases, the profiles become wider and their decay gets smoother. At even higher temperatures, where the dipole-dipole interactions are suppressed by thermal fluctuations, the filament brush is expected to have a parabolic density profile, as predicted for a non magnetic polymer brush.[47,48] The average brush height, shown in Figure 2b, reveals a non trivial dependence of the filament brush thickness on the temperature and the grafting density. At high temperature, the plateau of the equilibrium height is determined by the grafting density and, if the temperature starts decreasing, we can see that $\langle z^* \rangle$ slowly decreases from its saturation value. At approximately $T \sim 1.5$, the decrease of $\langle z^* \rangle$ with T changes significantly for both grafting densities, making it rather steep on further cooling. Importantly, as it was observed for the density profiles, in the region $T \sim [0.5, 1.5]$, $\langle z^* \rangle$ assumes basically the same values for both grafting densities.

In order to understand the origin of the non trivial dependence

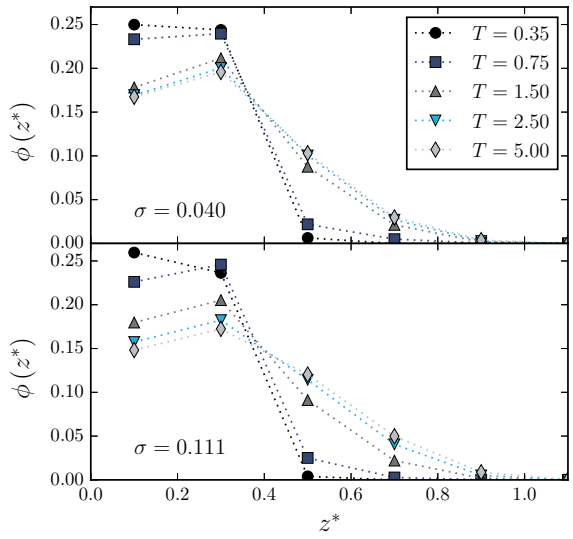

(a)

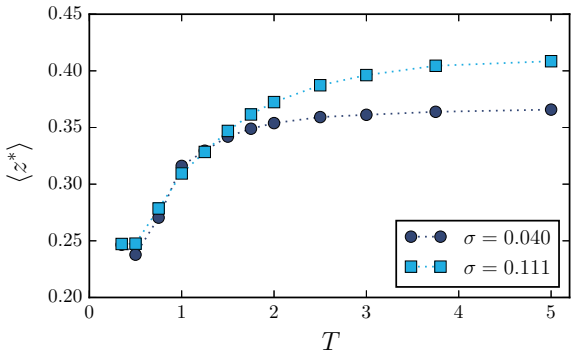

(b)

Fig. 2 Density profiles (a) and average brush heights (b) for different temperatures, grafting densities and zero external field.

of the equilibrium overall brush structure on the temperature and the grafting density, we applied the connectivity graph analysis described above to these simulation results. The distance criterion used here to define the generic connections between the magnetic colloids in the brush—and, with them, the connectivity graphs that represent the brush detailed structure—takes into account two different origins of pair formation. Besides the connectivity imposed by the filaments' permanent links, in general we can expect magnetic beads to self-assemble, forming close contact pairs whose relative orientations correspond to low energies of their dipole-dipole interaction. Due to its strongly directional nature, the part of the two dipoles' orientation phase space, corresponding to the attractive dipole-dipole pair interaction, is rather restricted. On the other hand, strong enough thermal fluctuations may force a pair of beads to come into close contact or to

separate regardless their relative dipole orientations. All magnetically and entropically driven non permanent connections, in addition to the permanent connections led by the crosslinkers along the filaments, can be taken into account by imposing a threshold centre-to-centre distance between connected beads equal to the maximum of the values $max(r_{\rm cut}, b_{\rm max})$, where $r_{\rm cut}$ is the cutoff distance defined for the soft core repulsion potential (1), $r_{\rm cut} = 2^{1/6}d$, and b_{max} is the maximum bond length observed for any pair of linked beads in the system at a given temperature. It should be noted that at high T one finds that $b_{max} > r_{\rm cut}$, whereas at low T this relationship is reversed. With this criterium, the first step in the connectivity analysis approach is to define the graphs that represent the connections and, from them, the clusters of filaments connected through their beads.

Figures 3 and 4 show a selection of snapshots of the brush equilibrium configurations obtained for different temperatures and the two sampled grafting densities. Next to each snapshot, the corresponding connectivity graph is also shown. In both snapshots and graphs, different clusters are identified by distinctive colours. For the lowest temperature, $T = 0.35$, and grafting density, $\sigma = 0.040$, one can see that the magnetic filament brush has a particular structure in which the permanent chains arch, connecting their free ends with the grafted or nearby end beads in neighbouring filaments. The topology of the corresponding connectivity graph also seems rather clear: all the beads are grouped into few clusters, in which the length of linear segments—*i.e.* segments without beads that have a degree higher than 2—is large. In most cases, such linear segments form closed paths. Due to the high correlation between the orientation of the dipoles and the chain backbone of the magnetic filaments we use—particularly strong at low T—the closed paths in the connectivity graphs indicate the existence of structures that tend to minimise their net magnetic moment, forming a nearly closed trajectory for the magnetic flux of their dipoles. For the higher σ, these general traits are even more pronounced: the whole brush is connected into a single cluster with a topology of multiple closed loops. Therefore, the structure of the brush at this temperature is clearly determined by the self-assembly of the filaments driven by the dipole-dipole interactions. At $T = 0.75$ the dipolar interaction is still very strong, but the entropic contribution starts ushering itself with the appearance of free chain ends, even though ring-like structures are still visible for low σ. In this T-region, one can also observe the formation of branched structures, which is more pronounced if the grafting density is high. At this point, it is useful to distinguish between two types of cluster topologies: the *linear chains*, that are formed by beads with a degree no higher than two, and the *branched structures*, in which there is at least one particle with a degree higher than two and/or the total amount of edges is equal or larger than the total amount of beads in the cluster. It is worth mentioning that, at $T \sim 1$, the branched structures contain mainly linear segments and do not have vertices with high degree, not even at $\sigma = 0.111$. To illustrate this, we calculated the distribution of values of vertex degrees averaged

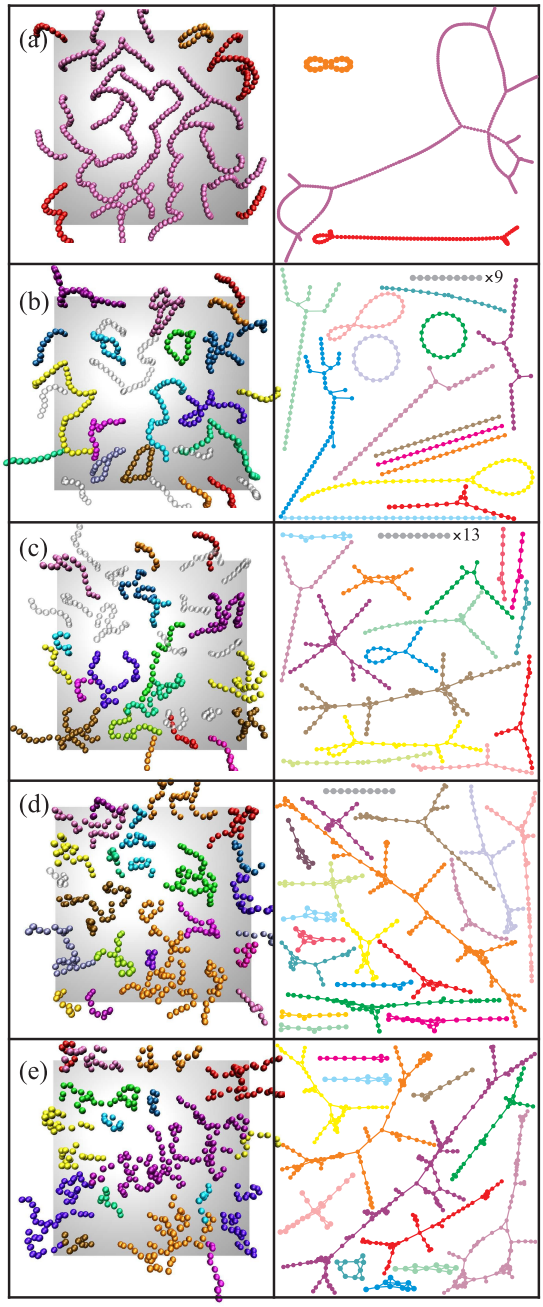

Fig. 3 Equilibrium configuration snapshots (left column, top view) and connectivity graphs (right column) at different temperatures for $\sigma = 0.040$, $H = 0$. Similar colours identify the same cluster in both, the snapshot and the corresponding graph. Grey colour indicates filaments without any non permanent connection. (a) $T = 0.35$. (b) $T = 0.75$. (c) $T = 1.5$. (d) $T = 2.5$. (e) $T = 3.75$.

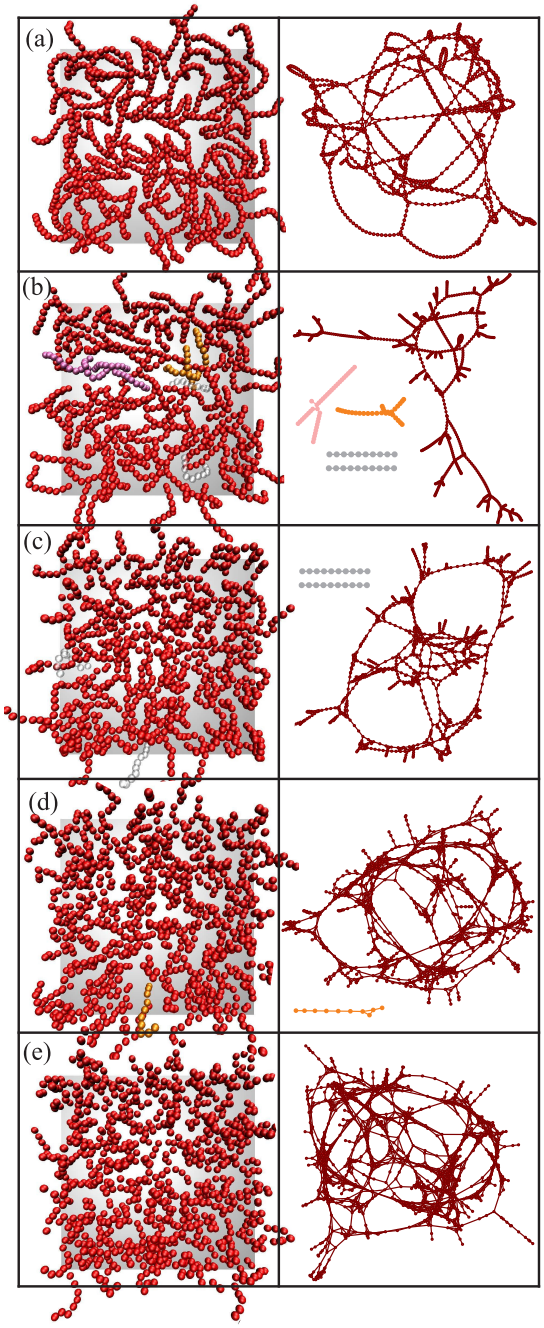

Fig. 4 Equilibrium configuration snapshots (left column, top view) and connectivity graphs (right column) at different temperatures for $\sigma = 0.111$, $H = 0$. Similar colours identify the same cluster in both, the snapshot and the corresponding graph. Grey colour indicates filaments without any non permanent connection. (a) $T = 0.35$. (b) $T = 0.75$. (c) $T = 1.5$. (d) $T = 2.5$. (e) $T = 3.75$.

over all sampled configurations. Figures 5a and 5b show 3D plots of such distributions for the two sampled grafting densities. One can see that up to $T_4 = 1$, the distributions are very narrow and have a clear maximum at $\delta = 2$. This corresponds to both the permanent connections between neighbours in the filaments and the connections between free and grafted ends in linear chain structures driven by the dipole-dipole interactions. The figures also evidence that, at higher temperatures, it becomes more probable to find branched structures for both values of grafting density, as the most frequent vertex degree tends to $\delta = 4$, for low grafting densities, and $\delta = 6$, if the brush is denser. As mentioned above, the directional character of the dipole-dipole interaction makes such types of multiple junctions unlikely. Consequently, one can conclude that, for temperatures above $T > 1$, the internal structure of the brush is mainly determined by thermal fluctuations. The structural changeover, driven by the change of T, is also clearly quantified by Figure 5c, where the fraction of particles in open chains and other structures as a function of the temperature is plotted. In this case, other structures include both branched ones and closed unbranched loops. For both systems, there is a clear minimum for the fraction of particles in these latter structures around $T \sim 1$. Below this temperature, the brush tends to be formed by closed loop structures with long linear segments. The fraction of particles in open chains is maximised at the temperature where the entropic gain of the chains' free ends is not anymore compensated for by the energetically favourable creation of an additional bond between them. If T increases further, the fraction of particles in branched structures begins to increase again due to the connections induced by the random thermal fluctuations. Finally, looking at the evolution with temperature of the sizes of the different cluster types, shown in Figure 5d, it becomes clear that, once the entropy loss associated with forming large zero-magnetic flux clusters is no longer feasible for the system, the cluster size reaches its minimum and then grows fast again due to simple entanglement caused by thermal motion. This also explains why the high temperature cluster size increase is much more pronounced for the brush with higher density.

The graph theory analysis used here allows us to not only characterise the overall structures of the clusters, but also to pinpoint how the bead position in a filament affects its part in the self-assembly. Here, in particular, we analyse the average betweenness of each particle in the brush at a given position along the filament for different temperatures, as shown in Figure 6. In this representation, the vertical axis corresponds to the positions along the filament, from the grafted end (in the bottom) to the free end (in the top), whereas the values of the betweenness for the two sampled grafting densities are shown in horizontal axes. The different values of the temperature are represented by the colours of the curves. As shown in our previous work,[19] for an individual chain, the average betweenness has a parabolic shape with maximum corresponding to the chain middle point. The higher the value of the average betweenness for a certain bead

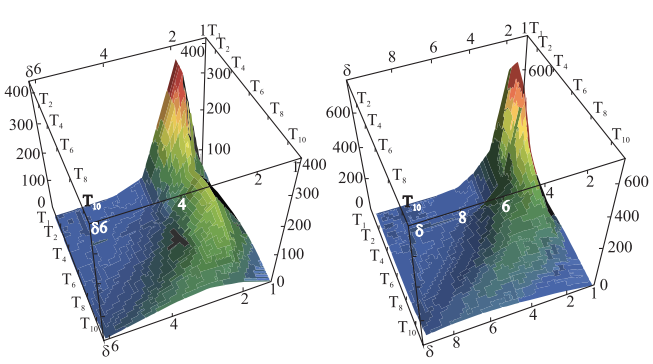

(a) $\sigma = 0.040$. (b) $\sigma = 0.111$.

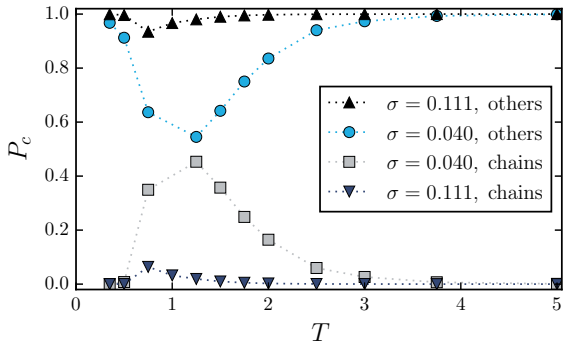

(c)

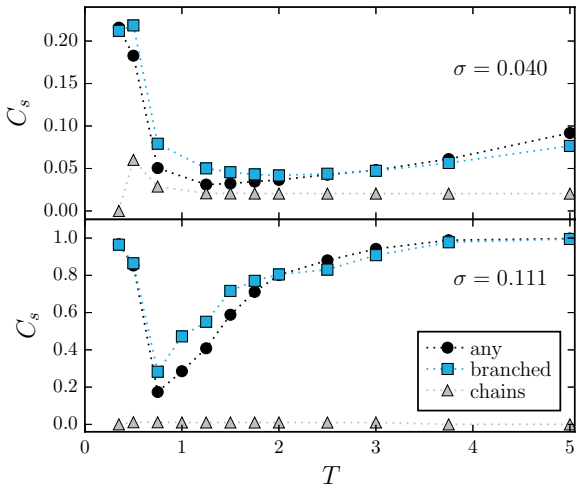

(d)

Fig. 5 Distributions of diverse cluster analysis parameters as a function of the temperature, obtained for different grafting densities and zero external field. (a), (b) Distributions of vertex degrees, δ. (c) Fraction of beads, P_c, belonging to chain-like or to any other type of clusters. (d) Distributions of average normalised cluster sizes, C_s, corresponding to branched, chain-like and any type of cluster structures.

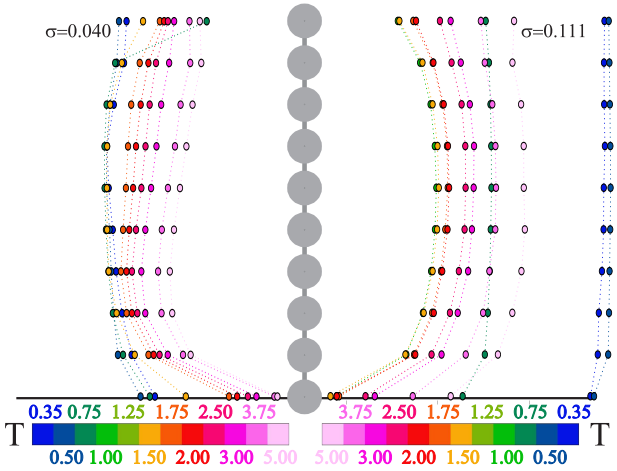

Fig. 6 Average betweenness in arbitrary units for the two sampled grafting densities (left and right horizontal scales), obtained for the different positions of the beads along the filaments (vertical scale). The grafted end corresponds to the lowest position, the free end to the upper one. The colours indicate the temperature corresponding to each curve.

position, the more active its participation in the path formation. In this way, Figure 6 completes our understanding of the structural changeover induced by the temperature. First, at low T, the active participation of the grafted ends in self-assembly is confirmed: as we can see, their betweenness is only slightly lower than that of free ends and middle particles for both values of σ. In general, a flat betweenness profile along the chain is the signature of loop formation. In this case, almost flat profiles are found for $\sigma = 0.111$ and $T \leq 0.75$. With growing temperature, the participation of grafted ends drops drastically. However, for $\sigma = 0.040$ the decrease of the grafted ends' betweenness is monotonous with T, whereas for the denser brush a reversal is observed at $T \sim 1.5$. This reversal for $\sigma = 0.111$ is also accompanied by the shift of the maximum betweenness to the beads closer to the grafted surface on heating. This tendency is much less pronounced for the brush with $\sigma = 0.040$, due to lower combinatoric probability of entanglement at high T. For both σ, the value of the betweenness of the free ends is rather high. For $\sigma = 0.111$, the betweenness of the free ends follows the reversal analogous to that of the grafted ends. Interestingly, this reversal, albeit on smaller scale, is also observed for free ends for the brush with $\sigma = 0.040$. The minimum of the betweenness of the free ends for the latter coincides with the maximum of particle fraction in chains, as seen in Figure 5c.

As a final conclusion, we underline that the interplay between entropy and energy in the constrained environment of a magnetic filament brush not only leads to a much broader range of temperature-induced self-assembly scenarios than that in non crosslinked dipolar particles, but also opens one possibility to efficiently tune the height and the local structure of such a brush. In

the next Section, we explore the use of external magnetic fields to also finely manipulate the brushes of magnetic filaments.

3.2 Effects of Normal External Magnetic Fields

Following the strategy used above, we first calculate the density profiles and average brush heights for both grafting densities at various values of an applied magnetic field, H, perpendicular to the grafting surface. Figure 7 shows the results for these parameters, obtained at $T = 1$. The most evident conclusion from the density profiles (Figure 7a) is that the grafting density has a strong influence on the response of the system to the field. For $\sigma = 0.040$, even a low field can perturb the brush and straighten the chains, hindering the formation of non permanent connections between the beads. This results in a flat rectangular density profile. For a denser brush, instead, the complex internal structure found at zero field at this temperature, discussed above, results to be less sensitive to the presence of the external field: only starting from $H = 3$, the density profile approaches a rectangular shape. To the same conclusion leads Figure 7b, where we plot the average height of the magnetic filament brush as a function of H. Here, for $\sigma = 0.111$, $\langle z^* \rangle$ grows significantly slower with an external field than that for $\sigma = 0.040$. At high fields, neither entropy nor dipolar interactions can compete with the field-dipole interaction, which leads to the alignement of the filaments with the field and, as a result, makes the brush average height reach its natural saturation for both values of σ. In order to start the characterisation of the brush structure at the scale of individual beads, we present in Figures 8 and 9 two sets of simulation snapshots and connectivity graphs analogous to the ones discussed in the Section above. In this case, the configurations correspond to selected values of the external field. A direct comparison of these plots with Figures 3 and 4 evidence a drastic difference with respect to the evolution with temperature. For low σ, the self-assembly between chains is almost completely hindered even by such a low field value as is $H = 0.5$. One can observe only few clusters, with a lot of linear segments, open ends and branching points with rather low degree. Importantly, this topology does not demand for a significant misalignment of the dipoles with respect to the field direction. If the field increases, the clusters gradually disappear, preserving in any case such characteristic topology. For higher σ and $H = 0.5$, instead, the clusters are rather big, with a relatively large amount of long linear segments. The junctions are rather versatile and free chain ends are present in a significant amount. The topology of the clusters in Figure 9a is very similar to the ones observed in Figures 4b and 4c. In other words, the influence of this low external magnetic field is negligible in this range of parameters. Besides that, the chains keep forming junctions even at high fields. The topology of these branched structures is not versatile and clearly coincides with the branched structures for $\sigma = 0.040$ and lower fields: multiple junctions are-

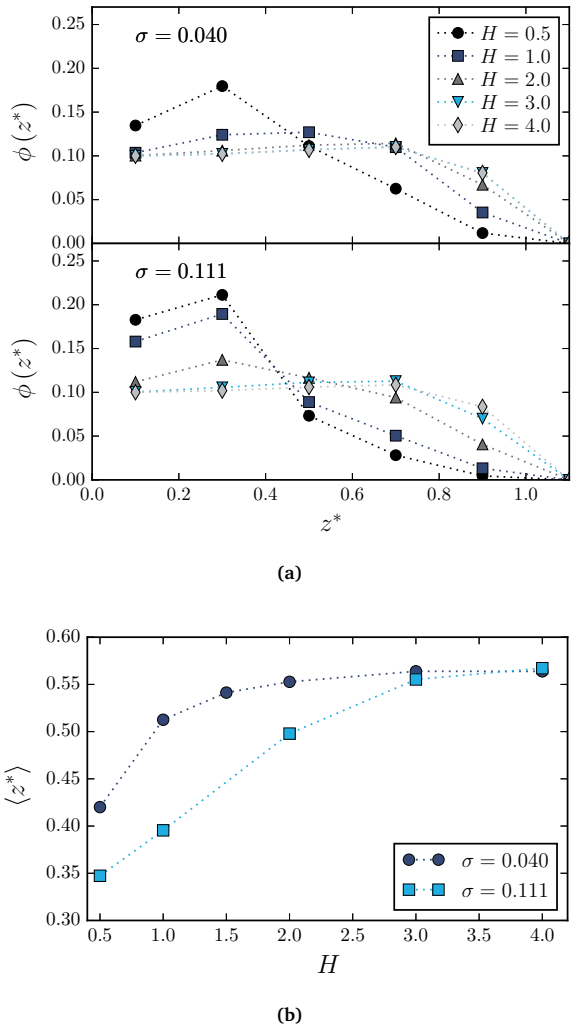

Fig. 7 Density profiles (a) and average brush heights (b) for different intensities of the external magnetic field and grafting densities, obtained at $T = 1$.

basically absent, whereas the amount of linear segments rapidly grows. A direct inspection of these configurations suggests that there are two typical branched structures compatible with an external magnetic field perpendicular to the grafting surface: X-type junctions, in which two nearly parallel filaments establish a single branching connection between beads located in their middle regions (see, for example, light blue clusters in Figure 9d), or half-interlaced chains with free ends, in which connected filaments twist around each other (see dark purple cluster in Figure 9d, for example). Looking for confirmation of the latter observation, we decided to focus on betweenness. This choice was driven by the fact that the distribution of degrees in this case provides very limited information, as it is very narrow and has a sharp peak at $\delta = 2$, due to the overwhelming dominance of linear segments.

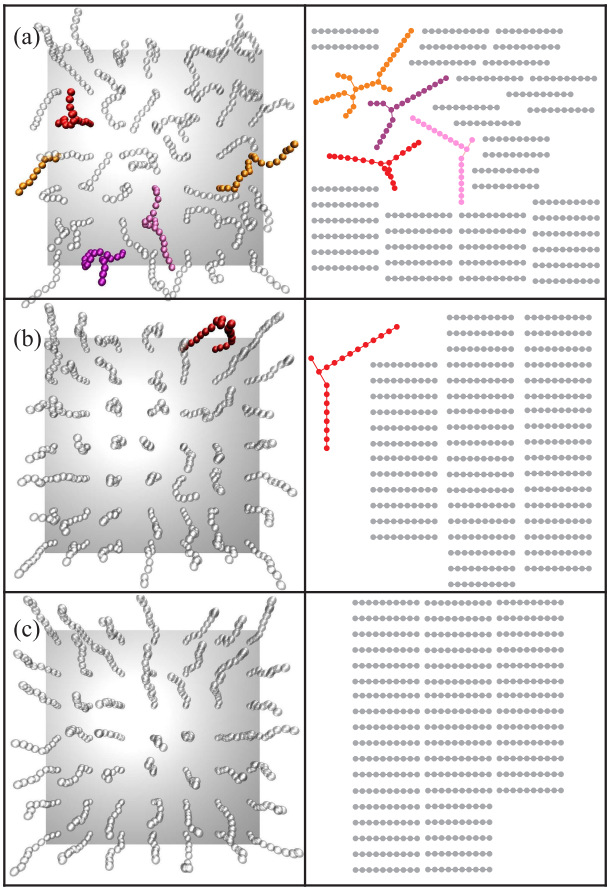

Fig. 8 Equilibrium configuration snapshots (left column) and connectivity graphs (right column) at different normal external fields for $\sigma = 0.040$, $T = 1$. (a) $H = 0.5$. (b) $H = 2$. (c) $H = 3$. For higher fields, no added connections were observed.

On the other hand, the average cluster size for both grafting densities is a monotonously decreasing function of the applied field, with a saturation value equal to the number of particles in a filament. If one plots the fractions of particles in chains and in branched structures, the chains contain almost all beads in the brushes starting from $H = 0.5$ for $\sigma = 0.040$ and from $H \sim 2.5$ for $\sigma = 0.111$. The betweenness, instead, can provide a more accurate measure after some manipulation. In our previous work, we showed that for a system of ideal N-particle chains—*i.e.*, chains with no other connections than the provided by the permanent links—the average betweenness as a function of the bead position along the filament, $j = \{1,\ldots,N\}$, can be written as: [19]

$$C_B^{id}(j) = -j^2 + j(N+1) - N. \qquad (9)$$

Thus, we can subtract $C_B^{id}(j)$ from the averaged betweenness of the beads given by Expression (8) to see even small deviations from the ideal system, $\Delta C_B(j) = C_B(j) - C_B^{id}(j)$. The results of this

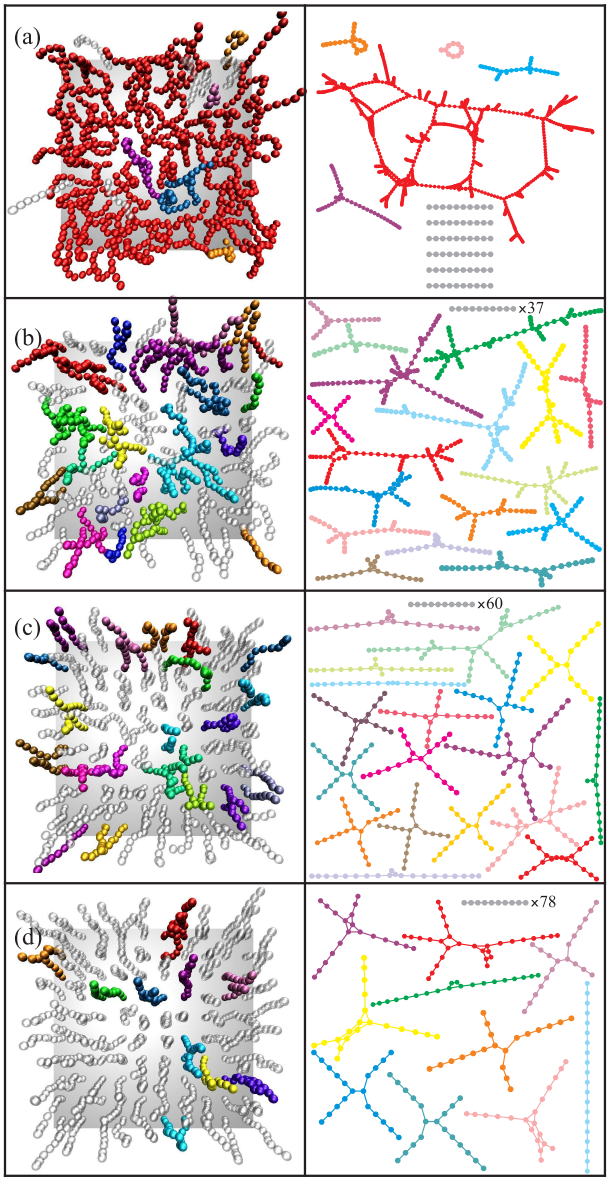

Fig. 9 Equilibrium configuration snapshots (left column) and connectivity graphs (right column) at different normal external fields for $\sigma = 0.111$, $T = 1$. (a) $H = 0.5$. (b) $H = 2$. (c) $H = 3$. (d) $H = 4$.

subtraction for high external fields are shown in Figure 10. For $\sigma = 0.040$ the deviations are basically negligible, but the position of the maximum clearly points towards the middle of the chain. The full confirmation of our aforementioned assumption about the topology of junctions can be obtained by looking at Figure 10. It becomes clear that the highest deviation from ideal chains is between particle numbers 5 and 6, with number 1 being the grafted end and number 10, the free chain end.

As a last comment, these kind of X-junctions have three clear

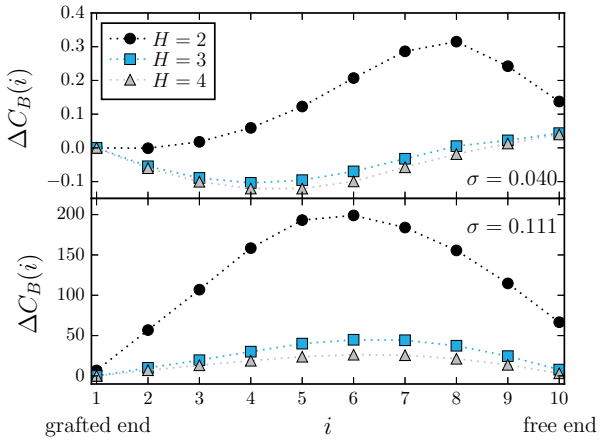

Fig. 10 Variation of the average centrality betweenness of the beads with respect to the case of an ideal chain, measured for two grafting densities as a function of the position of the bead along the filament.

advantages: they preserve the entropy of free chain ends, they add a negative dipolar connection, which lowers the system free energy, and basically do not perturb the dipoles aligned along the magnetic field. On the other hand, their presence lead to non-complete chain stretching at given fields.

4 Conclusions

In this work, we explored the control of the structural properties of a magnetic filament brush with the help of two external stimuli: temperature and an applied external magnetic field perpendicular to the grafting surface. Both parameters affect the self-assembly of magnetic colloids by changing the topology and the size distribution of formed clusters. The latter structural transformations manifest themselves in the brush density profiles and average brush height. In other words, we explored the possibility to manipulate the magnetic filament brush through fine tuning of the constituents' self-assembly. In order to carefully study the equilibrium properties of magnetic filament brushes, we employed the combination of molecular dynamics computer simulations and graph theory analysis methods. We investigated two grafting densities: $\sigma = 0.040$ and $\sigma = 0.111$. This allowed us to pinpoint the influence of chain concentration on the self-assembly. We showed that at zero field, low temperature and low grafting density, filament chains bend to connect their free ends to neighbouring grafted ends, creating a closed multi-ring-like cluster, whose magnetic moment is nearly zero. The same tendency, just with less regularity, is observed for high grafting density in zero-field at low-T regimes. Under these conditions, the brush is very compact, with a rather low height, and weakly magnetoresponsive. If the temperature grows slightly, the dipole-dipole interaction is still strong enough to drive to the self-assembly in long linear structures that involve both free and grafted chain ends, but the entropy leads to the opening of the magnetically closed structures, gaining in such a way the entropic contributions of the chains free ends. At this point the number of "chain-like" clusters reaches its maximum, and the number of branching points has its minimum. Further increase of T results in a completely random, highly branched network of bonds, mainly defined by the grafting density and thermal fluctuations. The analysis of the influence of the external field at $T = 1$ reveals a more drastic grafting density dependence. Thus, for low grafting density, even a low field leads to an almost complete elimination of the self-assembly between neighbouring chains and results in the brush formed by extended chains, whose length is the result of the competition between thermal fluctuations and dipole-dipole interaction stimulated by the external field. For high grafting density, instead, a weak external field cannot perturb the structures formed due to the dipolar interactions: the overall brush height remains rather small, and the brush continues to be rather dense up to moderate fields. For stronger fields, however, the same structural changeover, as observed for $\sigma = 0.040$ at low fields, takes place, and the filaments tend to straighten perpendicular to the grafting surface. We also observed that, even though the number of branching points decreases with the field, for $\sigma = 0.111$ there are two clear configurations of clusters that appear to "survive" even under strong external fields, namely, the X-shape junction connecting two neighbouring chains by only one point of their middle regions, and the staggered configuration of two chains. Both configurations do not demand large deviations of the dipoles from the orientation of the field. Cluster size is a monotonously decreasing function of the applied field. In general, the field response of the denser brush suggests the potential existence of a hysteresis-like behaviour on low-high-low field cycles. However, this effect deserves special attention and will be the subject of future studies. This work, instead, clearly shows that magnetic filament brushes have a complex microstructure with versatile self-assembly in clusters of different size and topology which, importantly, can be uniquely predicted, based on the grafting density, temperature, dipole moment and intensity of externally applied magnetic fields.

Even though at this point there is no direct experimental realisation of a magnetic filament brush, modern soft matter physics actually offers all necessary building blocks. Thus, for example, a very good control has been achieved in the synthesis of monodisperse magnetite or cobalt permanently magnetised nanoparticles.[5,49] On the other hand, growing experience in DNA origami[50,51] opens up a new perspective in precisely tuneable crosslinking. Finally, the recent advances in functionalisation of surfaces[12,52] provide various elaborated techniques to create an actual magnetic filament brush.

As a final comment, we briefly discuss the open questions that

arose during the study of field and temperature influence on the properties of the magnetic filament brush, which are far beyond the scope of this paper. First, it is important to understand the thermodynamics of these systems and analyse relevant parameters, like the specific heat, as a function of field and temperature. This can shed light on the differences between magnetic filament systems and self-assembling dipolar spheres brought by the presence of the permanent links. On the other hand, it is known that there is a series of structural transitions in dipolar hard spheres on cooling, but the temperatures at which they occur is rather low.[10,11] For the filament brush system, the temperature range should be extended in order to perform a proper analysis and provide an extensive comparison. Another control parameter, which is known to be very efficient in tuning brush properties, is the length of the grafted chains. Here, we purposefully focused on only one chain length to avoid multiple effects and provide a clear description of the structural transitions under cooling and increasing field. Now, one can easily separate the influence of the number of particles in filaments. Finally, an open question, which has already been mentioned above, is related to the external magnetic field: wether there exists a hysteresis on the increasing-decreasing field cycle and, if that is the case, what is the influence on it of the grafting density and the rest of brush parameters?

Acknowledgments

This research has been partially supported by the Austrian Research Fund (FWF): START-Projekt Y 627-N27. Authors are grateful to the Ural Federal University stimulating programme. S.S.K is supported by RFBR mol-a-ved 15-32-20549. E.V.N. acknowledges the support of President RF Grant No. MK-5216.2015.2. The authors are grateful to the Ministry of Education and Science of the Russian Federation (Contract 02.A03.21.000, Project 3.12.2014/K) and EU-Project 642774 ETN-Colldense. Computer simulations were performed at the Vienna Scientific Cluster (Austrian universities consortium for High Performance Computing) and the Nuredduna high-throughput computing cluster (IFISC, UIB-CSIC). J.J.C. and T.S. also acknowledge funding from a grant awarded by the Conselleria d'Innovació, Recerca i Turisme del Govern de les Illes Balears and the Europena Social Fund (ESF). We also thank Michaela McCaffrey for language suggestions.

References

1 G. M. Whitesides and B. Grzybowski, *Science*, 2002, **295**, 2418–2421.

2 R. Thiruvengadathan, V. Korampally, A. Ghosh, N. Chanda, K. Gangopadhyay and S. Gangopadhyay, *Reports on Progress in Physics*, 2013, **76**, 066501.

3 M. A. C. Stuart, W. T. S. Huck, J. Genzer, M. Muller, C. Ober, M. Stamm, G. B. Sukhorukov, I. Szleifer, V. V. Tsukruk, M. Urban, F. Winnik, S. Zauscher, I. Luzinov and S. Minko, *Nat Mater*, 2010, **9**, 101–113.

4 B. J. Park, F. F. Fang and H. J. Choi, *Soft Matter*, 2010, **6**, 5246–5253.

5 S. Singamaneni, V. N. Bliznyuk, C. Binek and E. Y. Tsymbal, *J Mater Chem*, 2011, **21**, 16819–16845.

6 M. Colombo, S. Carregal-Romero, M. F. Casula, L. Gutierrez, M. P. Morales, I. B. Bohm, J. T. Heverhagen, D. Prosperi and W. J. Parak, *Chem. Soc. Rev.*, 2012, **41**, 4306–4334.

7 M. Klokkenburg, C. Vonk, E. M. Claesson, J. D. Meeldijk, B. H. Erné and A. P. Philipse, *J Am Chem Soc*, 2004, **126**, 16706–16707.

8 M. Klokkenburg, R. P. A. Dullens, W. K. Kegel, B. H. Erné and A. P. Philipse, *Phys. Rev. Lett.*, 2006, **96**, 037203.

9 E. M. Furst and A. P. Gast, *Phys Rev Lett*, 1999, **82**, 4130–4133.

10 S. Kantorovich, A. O. Ivanov, L. Rovigatti, J. M. Tavares and F. Sciortino, *Phys. Rev. Lett.*, 2013, **110**, 148306.

11 S. S. Kantorovich, A. O. Ivanov, L. Rovigatti, J. M. Tavares and F. Sciortino, *Phys. Chem. Chem. Phys.*, 2015, **17**, 16601–16608.

12 A. C. Balazs, T. Emrick and T. P. Russell, *Science*, 2006, **314**, 1107–1110.

13 S. Behrens, *Nanoscale*, 2011, **3**, 877–892.

14 R. Dreyfus, J. Baudry, M. L. Roper, M. Fermigier, H. A. Stone and J. Bibette, *Nature*, 2005, **437**, 862–865.

15 J. J. Benkoski, S. E. Bowles, R. L. Jones, J. F. Douglas, J. Pyun and A. Karim, *J Polym Sci, Part B: Polym Phy*, 2008, **46**, 2267–2277.

16 K. Ērglis, D. Zhulenkovs, A. Sharipo and A. Cēbers, *J Phys-Condens Mat*, 2008, **20**, 204107.

17 Z. Zhou, G. Liu and D. Han, *ACS Nano*, 2009, **3**, 165–172.

18 J. Byrom, P. Han, M. Savory and S. L. Biswal, *Langmuir*, 2014, **30**, 9045–9052.

19 P. A. Sánchez, E. S. Pyanzina, E. V. Novak, J. J. Cerdà, T. Sintes and S. S. Kantorovich, *Macromolecules*, 2015, DOI: 10.1021/acs.macromol.5b01086.

20 S. T. Milner, *Science*, 1991, **251**, 905–914.

21 A. Halperin, M. Tirrell and T. Lodge, in *Macromolecules: Synthesis, Order and Advanced Properties*, Springer Berlin Heidelberg, 1992, vol. 100/1, pp. 31–71.

22 F. Zhou and W. T. S. Huck, *Phys. Chem. Chem. Phys.*, 2006, **8**, 3815–3823.

23 W. S. Choi, H. Y. Koo, J. Y. Kim and W. T. S. Huck, *Advanced Materials*, 2008, **20**, 4504–4508.

24 Y. Ye, Z. Pan, L. Zhang, L. He, A. Xia and H. Liang, *Journal of Polymer Science Part B: Polymer Physics*, 2010, **48**, 1873–1881.

25 H. Singh, P. E. Laibinis and T. A. Hatton, *Nano Lett*, 2005, **5**,

2149–2154.
26 A. Cēbers, *Curr Opin Colloid Interface Sci*, 2005, **10**, 167–175.
27 M. Belovs and A. Cēbers, *Phys Rev E*, 2009, **79**, 051503.
28 F. Fahrni, M. W. J. Prins and L. J. van IJzendoorn, *Lab Chip*, 2009, **9**, 3413–3421.
29 A. Babataheri, M. Roper, M. Fermigier and O. D. Roure, *Journal of Fluid Mechanics*, 2011, **678**, 5–13.
30 I. Javaitis and V. Zilgalve, *Adv Mat Res*, 2011, **222**, 221–224.
31 Y. N. Kaznessis, D. A. Hill and E. J. Maginn, *Macromolecules*, 1998, **31**, 3116–3129.
32 J. J. Cerdà, P. A. Sánchez, T. Sintes and C. Holm, *Soft Matter*, 2013, **9**, 7185–7195.
33 P. A. Sánchez, J. J. Cerdà, T. Sintes, A. O. Ivanov and S. S. Kantorovich, *Soft Matter*, 2015, **11**, 2963–2972.
34 J. D. Weeks, D. Chandler and H. C. Andersen, *J Chem Phys*, 1971, **54**, 5237–5247.
35 F. F. Abraham and Y. Singh, *J Chem Phys*, 1977, **67**, 2384–2385.
36 M. P. Allen and D. J. Tildesley, *Computer Simulation of Liquids*, Clarendon Press, Oxford, 1st edn., 1987.
37 J. J. Cerdà, V. Ballenegger, O. Lenz and C. Holm, *J Chem Phys*, 2008, **129**, 234104.
38 A. Bródka, *Chem Phys Lett*, 2004, **400**, 62–67.
39 H. J. Limbach, A. Arnold, B. A. Mann and C. Holm, *Comput Phys Commun*, 2006, **174**, 704–727.
40 A. Arnold, O. Lenz, S. Kesselheim, R. Weeber, F. Fahrenberger, D. Roehm, P. Košovan and C. Holm, in *Meshfree Methods for Partial Differential Equations VI*, ed. M. Griebel and M. A. Schweitzer, Springer Berlin Heidelberg, 2013, vol. 89, pp. 1–23.
41 C. Godsil and G. Royle, in *Algebraic Graph Theory*, Springer New York, 2001, vol. 207, pp. 163–192.
42 G. Zanchetta, F. Giavazzi, M. Nakata, M. Buscaglia, R. Cerbino, N. A. Clark and T. Bellini, *Proceedings of the National Academy of Sciences*, 2010, **107**, 17497–17502.
43 C. De Michele, L. Rovigatti, T. Bellini and F. Sciortino, *Soft Matter*, 2012, **8**, 8388–8398.
44 A. Lebedev, *Colloid Journal*, 2010, **72**, 815–819.
45 A. Lebedev and S. Lysenko, *J. Magn. Magn. Mater.*, 2011, **323**, 1198–1202.
46 P. A. Sánchez, J. J. Cerdà, T. Sintes and C. Holm, *J. Chem Phys.*, 2013, **139**, 044904.
47 M. Murat and G. S. Grest, *Macromolecules*, 1989, **22**, 4054–4059.
48 S. T. Milner, T. A. Witten and M. E. Cates, *Macromolecules*, 1988, **21**, 2610–2619.
49 J. Liu, *JOM-J Min Met Mat S*, 2010, **62**, 56–61.
50 S. Srivastava, D. Nykypanchuk, M. Fukuto, J. D. Halverson, A. V. Tkachenko, K. G. Yager and O. Gang, *Journal of the American Chemical Society*, 2014, **136**, 8323–8332.
51 R. M. Zadegan and M. L. Norton, *International Journal of Molecular Sciences*, 2012, **13**, 7149–7162.
52 O. Azzaroni, *Journal of Polymer Science Part A: Polymer Chemistry*, 2012, **50**, 3225–3258.